NUCL SCI TECH (2020) 31:71
https://doi.org/10.1007/s41365-020-00779-6

Examination of an isospin-dependent single-nucleon momentum distribution for isospin-asymmetric nuclear matter in heavy-ion collisions

Gao-Feng Wei[1,2] · Qi-Jun Zhi[1,2] · Xin-Wei Cao[3] · Zheng-Wen Long[4]

Received: 5 March 2020 / Revised: 14 April 2020 / Accepted: 15 April 2020 / Published online: 26 June 2020

Abstract Within a transport model using nucleon momentum profiles as the input from a parameterized isospin-dependent single-nucleon momentum distribution, with a high momentum tail induced by short-range correlations, we employ ^{197}Au + ^{197}Au collisions at 400 MeV/nucleon to examine the effects of the short-range correlations on the pion and flow observables in probing the nuclear symmetry energy. We investigate how reliable this isospin-dependent single-nucleon momentum distribution is and determine the corresponding parameter settings. Apart from the significant effects of the short-range correlations on the pion and flow observables that are observed, we also find that the theoretical simulations of the ^{197}Au + ^{197}Au collisions with this momentum distribution using two sets of parameters, extracted from the experimental analysis and the self-consistent Green's function prediction, can reproduce the neutron elliptic flows of the FOPI-LAND experiment and the π^-/π^+ ratios of the FOPI experiment, respectively, under the symmetry energy setting in a particular range. Therefore, we conclude that this parameterized isospin-dependent single-nucleon momentum distribution is reliable for isospin-asymmetric nuclear matter. Correspondingly, two sets of parameters extracted from both the experimental analysis and the self-consistent Green's function prediction cannot be excluded according to the available experimental information at present.

Keywords Single-nucleon momentum distribution · Isospin-asymmetric nuclear matter · Short-range correlations · Heavy-ion collisions · Symmetry energy

1 Introduction

The determination of the equation of state (EoS) of dense isospin-asymmetric nuclear matter (IANM) is a fascinating problem in nuclear physics and nuclear astrophysics, owing to its vital importance in studying the structure of radioactive nuclei and the evolution of compact stars. This topic has thus attracted significant attention in the past few decades; see Refs. [1, 2] for recent comprehensive reviews. The predictions of the EoS of dense IANM, particularly its density-dependent symmetry energy term, are still discrepant, even controversial, at the suprasaturation density [3–5]; however, many isospin signals have been proposed, with the aim of detecting the EoS of dense IANM Refs. [1, 2, 6, 7]. This is primarily because the isovector part of the nuclear interactions is significantly weaker than the isoscalar part; thus, these isospin signals

This work was supported by the National Natural Science Foundation of China (Nos. 11965008, 11405128,and U1731218), Guizhou Provincial Science and Technology Foundation (No. [2020]1Y034), the PhD-funded project of Guizhou Normal university (No. GZNUD[2018]11), and the Xi'an Science and Technology Planning project (No. CXY1531WL35).

✉ Gao-Feng Wei
wei.gaofeng@gznu.edu.cn

[1] School of Physics and Electronic Science, Guizhou Normal University, Guiyang 550025, China

[2] Guizhou Provincial Key Laboratory of Radio Astronomy and Data Processing, Guizhou Normal University, Guiyang 550025, China

[3] School of Mechanical and Material Engineering, Xi'an University of Arts and Sciences, Xi'an 710065, China

[4] College of Physics, Guizhou University, Guiyang 550025, China

can typically be interfered by other factors in theoretical simulations and experimental measurements. Therefore, some attempts on strategic studies [8] and covariance analyses [9] of these isospin observables, as well as some comparative projects [10] between different theoretical communities, have been done to understand the origin of these discrepancies. Alternatively, some studies on the deficiency of the mechanism itself in theoretical simulations also present the correct direction to the solution of these discrepancies, for example, the pion potential [11–13] and the Δ isovector potential [14, 15] have been confirmed to interfere with the sensitivity of the π^-/π^+ ratio in probing the nuclear symmetry energy using heavy-ion collisions (HICs).

The momentum distribution of nucleons in a nuclear system, as the direct reflection of strong interactions at short distances, is a long-standing interest in nuclear physics [16, 17]. In particular, the discovery of correlated nucleons pairs in a ^{12}C nucleus in high energy electron scattering experiments at the Jefferson Laboratory (JLab) [16] aroused higher enthusiasm in studying the momentum distribution of nucleons and their short-range correlations (SRCs) in the past decades; see Refs. [17, 18] for comprehensive reviews. Qualitatively, some general knowledge on the nucleon momentum distribution (NMD) has been gained, i.e., the tensor component of nuclear interactions can typically push a few nucleons from low to high momentum, leading to a high momentum tail (HMT) above the nucleon Fermi momentum $k_{\rm F}$ and a corresponding low momentum depletion (LMD) below the $k_{\rm F}$ in the NMD [17, 18]. Moreover, a qualitative consensus of the *np* dominance of SRC pairs in the HMT has been reached by various theoretical and experimental investigations [19–22]. Quantitatively, the experimental analyses at the JLab suggest that approximately 20% of nucleons are in the HMT of a nucleus, from light ^{12}C [16] to heavy ^{208}Pb [22, 23]. Moreover, the systematic analyses of these results from the experiments at the JLab indicate that the fraction of nucleons in the HMT is approximately 25% in the symmetric nuclear matter (SNM) at the saturation density ρ_0 [24]. However, the theoretical calculations begin to deviate significantly from this suggested fraction for the HMT in the SNM at ρ_0. For example, the self-consistent Green's function (SCGF) approach, employing the Av18 interaction, predicts that only 11–13% of nucleons are in the HMT for the SNM at ρ_0; however, a higher fraction of 4–5% of nucleons are in the HMT for the pure neutron matter (PNM) at ρ_0 [25].The Bruckner-Hartree-Fock calculations go so far as to suggest a wide range for nucleons in the HMT in the SNM at ρ_0, from approximately 10%, using the N3LO450 interaction, to approximately 20%, using the Av18, Paris, or Nij93 interactions [26].

Recently, guided by the aforementioned studies, a parameterized isospin-dependent single NMD, with an HMT induced by SRCs, i.e.,

$$n_{\mathbf{k}}^{J}(\rho,\delta)=\begin{cases}\Delta_J+\beta_J I\left(|\mathbf{k}|/k_{\rm F}^{J}\right), & 0<|\mathbf{k}|\le k_{\rm F}^{J},\\ C_J\left(k_{\rm F}^{J}/|\mathbf{k}|\right)^4, & k_{\rm F}^{J}<|\mathbf{k}|\le \phi_J k_{\rm F}^{J},\end{cases} \tag{1}$$

was proposed for the IANM [18, 27]. Here, the parameters Δ_J and β_J characterize, respectively, the depletion of the Fermi sphere at zero momentum and the strength of momentum-dependent depletion through the momentum-dependent function $I(|\mathbf{k}|/k_{\rm F}^{J})\approx(|\mathbf{k}|/k_{\rm F}^{J})^2$ in the range of $0<|\mathbf{k}|\le k_{\rm F}^{J}$, with $k_{\rm F}^{J}=(3\pi^2\rho_J)^{1/3}$, where the index J denotes protons or neutrons. The parameters C_J and ϕ_J are the amplitude and cutoff value of the high momentum distribution, respectively; all four parameters can be expressed in isospin asymmetry δ in the general form of $Y_J=Y_0(1+Y_1\tau_3^J\delta)$, with τ_3^n as 1 for neutrons and τ_3^p as -1 for protons. It should be mentioned that the normalization condition $[2/(2\pi)^3]\int_0^\infty n_{\mathbf{k}}^{J}(\rho,\delta)\mathrm{d}\mathbf{k}=\rho_J=(k_{\rm F}^{J})^3/3\pi^2$ requires that only three of these four parameters are independent; therefore, one can use C_J, ϕ_J, and β_J as the independent parameters, as in Refs. [18, 27]. Moreover, to approximately cover the recent experimental findings [22, 24] and the SCGF calculations [25], the studies in Refs. [18, 27] extracted two sets of parameters: One is the HMT-SCGF parameter, i.e., $C_0=0.121$, $C_1=-0.01$, $\phi_0=1.49$, $\phi_1=-0.25$, and $\beta_0=\beta_1=0$, which leads to a fraction of the total nucleons, approximately 12.6% in the HMT, in a finite ^{197}Au nucleus at ρ_0 and the corresponding fractions of high-momentum protons and neutrons over total protons and neutrons are approximately 15% and 11%, respectively; Another is the HMT-exp. parameter, i.e., $C_0=0.161$, $C_1=-0.25$, $\phi_0=2.38$, $\phi_1=-0.56$, $\beta_0=-0.27$, and $|\beta_1|\le 1$, which leads to a fraction of total nucleons, approximately 25.2% in the HMT, in a finite ^{197}Au nucleus at ρ_0 and the individual fractions of high-momentum protons and neutrons are approximately 30% and 22%, respectively. For more details about this isospin-dependent NMD, we refer readers to Refs. [18, 27].

2 The model

2.1 Initialization of the model

The present study is carried out in the framework of an isospin- and momentum-dependent Boltzmann–Uehling–Uhlenbeck (IBUU) transport model [28]. As the first step,

the startup of the IBUU model is the initialization of colliding nuclei in the coordinate and momentum spaces. To initialize the finite ^{197}Au nucleus in the momentum space, we have transformed the above NMD for the IANM into that for the finite ^{197}Au nucleus, using the local-density approximation [29]. The specific distributions generated from the initialization in our reaction model are shown in Fig. 1. Consistent with the previous theoretical results [19–21, 30] and the recent experimental evidence [23], a higher fraction of high-momentum protons than that of neutrons, in a neutron-rich nuclear system, results from the *np* dominance of SRC pairs in the HMT. Moreover, except for the observed LMD below the $k_{\rm F}$ and the corresponding HMT above the $k_{\rm F}$, the nucleon momentum profiles generated from this isospin-dependent NMD are very similar to those without the consideration of SRCs, thus, preliminarily indicating the feasibility of initialization using this isospin-dependent NMD in the momentum space. Certainly, the reliability of specific parameter settings based on this distribution still requires verification, as shown in the following parts. Additionally, because the fraction of high-momentum nucleons calculated with the HMT-exp. parameter is higher than that in the calculations with the HMT-SCGF parameter, a more apparent LMD below the $k_{\rm F}$, and the corresponding HMT above the $k_{\rm F}$, can be observed in calculations with the HMT-exp. parameter. Therefore, some sensitive observables of the NMD are expected to reflect these differences in ^{197}Au+^{197}Au collisions. Moreover, we have also checked the effects of the value β_1 in the allowed range on the NMD in the ^{197}Au nucleus and found that the NMD of the ^{197}Au nucleus is less influenced by the value of the β_1 parameter. Thus, we randomly choose the value for β_1 in the allowed range in this study.

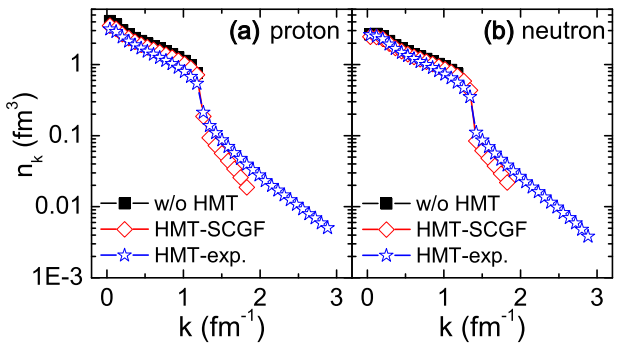

Fig. 1 (Color online) Momentum distributions of **a** protons and **b** neutrons in the initial ^{197}Au nucleus, with and without the consideration of SRCs. The normalization condition $[2/(2\pi)^3]\int_0^\infty n_{\mathbf{k}}^J(\rho,\delta)d\mathbf{k}=\rho_J=(k_{\rm F}^J)^3/3\pi^2$ is used

2.2 Interaction used in the model

For the nuclear interaction used in the present study, we take the form similar to our recent work [31, 32] because this nuclear interaction has considered details that are more reasonable, including distinguishing the density dependencies of in-medium *nn*, *pp*, and *np* interactions in the effective many-body force term [33], as well as fitting the high-momentum behaviors of the nucleon optical potential extracted from nucleon-nucleus-scattering experiments [34]. Specifically, the nuclear interaction used in this study is expressed as

$$\begin{aligned}U(\rho,\delta,\vec{p},\tau)=&A_{\rm u}(x)\frac{\rho_{-\tau}}{\rho_0}+A_{\rm l}(x)\frac{\rho_\tau}{\rho_0}+\frac{B}{2}\left(\frac{2\rho_\tau}{\rho_0}\right)^\sigma(1-x)\\&+\frac{2B}{\sigma+1}\left(\frac{\rho}{\rho_0}\right)^\sigma(1+x)\frac{\rho_{-\tau}}{\rho}\left[1+(\sigma-1)\frac{\rho_\tau}{\rho}\right]\\&+\frac{2C_{\rm l}}{\rho_0}\int d^3p'\frac{f_\tau(\vec{p}')}{1+(\vec{p}-\vec{p}')^2/\Lambda^2}\\&+\frac{2C_{\rm u}}{\rho_0}\int d^3p'\frac{f_{-\tau}(\vec{p}')}{1+(\vec{p}-\vec{p}')^2/\Lambda^2},\end{aligned}\tag{2}$$

and the corresponding like-type and unlike-type parameters $A_{\rm l}(x)$ and $A_{\rm u}(x)$ are expressed in forms of

$$A_{\rm l}(x)=A_{\rm l0}-\frac{2B}{\sigma+1}\left[\frac{(1-x)}{4}\sigma(\sigma+1)-\frac{1+x}{2}\right],\tag{3}$$

$$A_{\rm u}(x)=A_{\rm u0}+\frac{2B}{\sigma+1}\left[\frac{(1-x)}{4}\sigma(\sigma+1)-\frac{1+x}{2}\right].\tag{4}$$

The parameter x embedded in the above expressions mimics the slope value $L\equiv 3\rho(dE_{\rm sym}/d\rho)$ of the nuclear symmetry energy at ρ_0, predicted by various many-body theories, without changing the value of the nuclear symmetry energy $E_{\rm sym}(\rho)$ at ρ_0 and any properties of the SNM. Generally, without the consideration of correlations in a nuclear system, the kinetic part of the nuclear symmetry energy is calculated from the free Fermi gas model as $E_{\rm sym}^{\rm kin}(\rho)=8\pi p_{\rm f}^5/9mh^3\rho\approx 12.5(\rho/\rho_0)^{2/3}$, with Fermi momentum $p_{\rm f}=\hbar(3\pi^2\rho/2)^{1/3}$. Because the SRCs significantly reduce the $E_{\rm sym}^{\rm kin}(\rho)$, according to some microscopic calculations [30, 35] and experimental studies [22, 24], we need to modify this expression. As was indicated in Ref. [30], what we identify as correlation driven is the reduction of $E_{\rm sym}^{\rm kin}(\rho)$; therefore, the $E_{\rm sym}^{\rm kin}(\rho)$ is the sole criterion that can guide one to incorporate the SRC effects into nuclear effective interactions phenomenologically. To this end, we readjust the parameters of the nuclear interactions to phenomenologically incorporate the SRC effects into nuclear effective interactions for the SRC scenario.

Table 1 The parameters used in the present study

Parameters	W/o HMT	With HMT
$A_{\mathrm{l}0}$ (MeV)	− 96.963	− 96.963
$A_{\mathrm{u}0}$ (MeV)	− 36.963	− 36.963
C_{l} (MeV)	− 40.820	− 24.719
C_{u} (MeV)	− 119.368	− 135.469
B (MeV)	141.963	141.963
σ	1.2652	1.2652
Λ/p_{f}	2.424	2.424

Moreover, considering that only a minority of nucleons are SRC correlated, we assume that the kinetic symmetry energy also holds for the 2/3 regularity, with respect to densities. According to a microscopic calculation [35], the symmetry energy at ρ_0 is almost from its potential part. It is for this reason that we employ the expression $E_{\mathrm{sym}}^{\mathrm{kin}}(\rho) = 12.5\left[(\rho/\rho_0)^{2/3} - 1\right]$ for the kinetic symmetry energy to meet this demand for the SRC scenario, similar to the previous study [36]. Using empirical constraints on the properties of symmetric and/or asymmetric nuclear matter at $\rho_0 = 0.16$ fm^{-3} (see, Ref. [37] for the detailed constraints used in this study) we have fitted the parameters of the nuclear interactions, i.e., $A_{\mathrm{l}0}$, $A_{\mathrm{u}0}$, B, C_{l}, C_{u}, σ, and Λ, for the scenarios without and with SRCs, respectively. Specifically, the values of two sets of parameters, denoted as "w/o HMT" and "with HMT," are shown in Table 1.

Obviously, the isoscalar potentials $U_0(\rho, p)$ under the consideration of SRCs are completely identical with those without, at either low densities or high densities, because only the symmetry energy is used as the criterion of the correlation-driven effects. As a result, the corresponding EoS of the SNM are completely identical to each other in these scenarios, as shown in Fig. 2. As indicated in Eq. (34) of Ref. [33], the EoS of SNM is actually involved in the combination of parameters C_{l} and C_{u}, instead of their individual values, i.e., $C_{\mathrm{l}} + C_{\mathrm{u}}$; therefore, the SRCs will naturally not affect the EoS of SNM at either low densities or high densities. However, the symmetric potentials with the consideration of SRCs will begin to deviate significantly from those without. Naturally, through decomposing the single-nucleon potential in Eq. (2), i.e., $U_{p,n}(\rho, \delta, p) \approx U_0(\rho, p) + U_{\mathrm{sym}}(\rho, p)(\tau\delta)$, with $\tau = 1$ for neutrons and -1 for protons, one can find that the nuclear interaction in Eq. (2) employing the "with HMT" parameter is essentially different from that with the "w/o HMT" parameter, although an identical expression of nuclear interactions in form is used in these two different scenarios. In principle, for the SRC scenarios, but for different initialization, i.e., the HMT-SCGF parameter and HMT-exp.

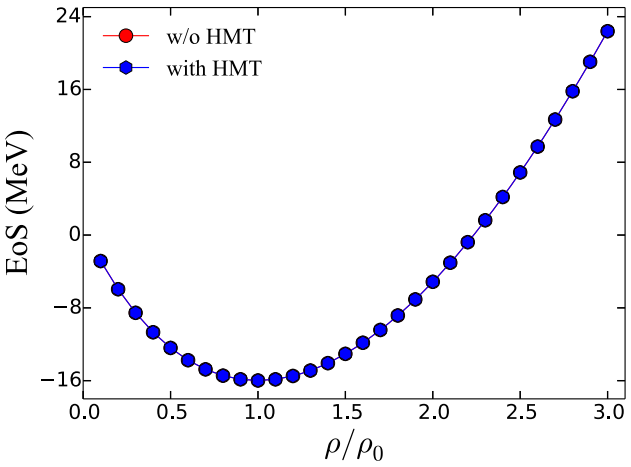

Fig. 2 (Color online) EoS of symmetric nuclear matter calculated with (blue solid hexagon) and without (Red solid circle) the consideration of SRCs

parameter, we should exactly fit the different nuclear interaction parameters according to the different fractions of SRC nucleons, instead of using an identical interaction parameter, i.e., the "with HMT" parameter. However, the quantitative results regarding this issue are still inconclusive, according to present microscopic calculations [30, 35]. Owing to what we can identify as correlation driven is the reduction of $E_{\mathrm{sym}}^{\mathrm{kin}}(\rho)$ [30]; therefore, $E_{\mathrm{sym}}^{\mathrm{kin}}(\rho)$ is the sole criterion that can guide one to incorporate the SRC effects into nuclear effective interactions phenomenologically. However, considering the fact that the shapes of NMD for these two cases are similar to each other, their differences are only the initial maximum momentum and the specific fraction of high-momentum nucleons; therefore, the utilization of identical nuclear interactions in form for these two cases is suitable at the level of the mean field. It should be emphasized that the initialization effects, and thus, the resulting differences of the initial maximum momentum of SRC nucleons, as well as their fractions in these two cases, will also be incorporated into the dynamics process of the reactions through the momentum dependent C_{l} and C_{u} integral terms.

Instead of the traditional Coulomb field used in the theoretical simulations of nucleus–nucleus collisions, the Liénard–Wiechert formulae [38, 39] are also used for the relativistic calculations of electromagnetic interactions created by fast-moving charged particles during HICs in the present study, i.e.,

$$e\vec{E}(\vec{r}, t) = \frac{e^2}{4\pi\varepsilon_0} \sum_n Z_n \frac{c^2 - v_n^2}{\left(cR_n - \vec{R}_n \cdot \vec{v}_n\right)^3} \left(c\vec{R}_n - R_n\vec{v}_n\right), \quad (5)$$

$$e\vec{B}(\vec{r},t) = \frac{e^2}{4\pi\varepsilon_0}\sum_n Z_n \frac{c^2 - v_n^2}{(cR_n - \vec{R}_n\cdot\vec{v}_n)^3}\vec{v}_n \times \vec{R}_n, \quad (6)$$

because they can also significantly affect some isospin observables, such as the π^-/π^+ ratio and the neutron–proton differential transverse flow in HICs at intermediate energies, especially at approximately 400 MeV/nucleon, see Refs. [31, 32] for more details. Moreover, to improve the accuracies of the theoretical simulations of HICs, we have also considered the pion potential and the Δ isovector potential in the present study. Specifically, when the pionic momentum is higher than 140 MeV/c, we adopt the pion potential based on the Δ-hole model, of the form used in Ref. [40]; when the pionic momentum is lower than 80 MeV/c, we use the pion potential of the form used in Refs. [41–43], while for the pionic momentum in the range from 80–140 MeV/c, an interpolative pion potential constructed by O. Buss in Ref. [40] is used. For the effects of this pion potential on the isospin observables, such as the π^-/π^+ ratio in HICs, we refer readers to Ref. [12] for more details. For the Δ potential, guided by the earlier studies [14, 15] and according to the decay mechanism of Δ resonances, we use an isospin-dependent Δ potential in the present study, i.e.,

$$U(\Delta^{++}) = f_\Delta U(p), \quad (7)$$

$$U(\Delta^{+}) = f_\Delta\left[\frac{1}{3}U(n) + \frac{2}{3}U(p)\right], \quad (8)$$

$$U(\Delta^{0}) = f_\Delta\left[\frac{2}{3}U(n) + \frac{1}{3}U(p)\right], \quad (9)$$

$$U(\Delta^{-}) = f_\Delta U(n). \quad (10)$$

The quantitative results of the Δ potential are still inconclusive at present; however, considering that the depth of the nucleon potential is approximately − 50 MeV, while that of the Δ potential is empirically constrained around − 30 MeV, we additionally introduce an identical factor $f_\Delta = 2/3$ for them to meet this demand, even though this factor may be different for the Δ resonances with different charged states.

3 Results and discussions

Before presenting the results of our study, we first examine the emission time and emission rate of nucleons during collisions to verify the stability of our model. To this end, we use the criterion of the last strong interaction to calculate the average emission time and emission rate for nucleons in the target of the ^{197}Au + ^{197}Au collisions, without distinguishing the proton and neutron. Statically, the presence of nucleons with a momentum greater than k_F in the initial target will naturally cause an increase in nucleon emissions in the initial reaction stage, owing to the larger pressure generated in the collision region by these high-momentum nucleons and their violent collisions. The effects of the correlations between these nucleons will cause a corresponding reduction of nucleon emissions to compete with the former. However, at the initial reaction stage, the effect of the former will dominate. As expected, for nucleons with a momentum greater than approximately 600 MeV/c, their average emission time shows sensitivities to the fraction of SRC nucleons, as shown in panel (a) of Fig. 3, i.e., compared to cases excluding and/or including fewer SRC nucleons in the target, the case including more SRC nucleons in the colliding nuclei gets the preequilibrium nucleons with faster emission. Additionally, as shown in panel (b) of Fig. 3, the nucleon emission rate before approximately 27 fm/c shows a larger value in SRC scenarios, in particular, for that with the HMT-exp. parameter. This implies that more SRC nucleons in the target cause more nucleons emitted in this period. At the early reaction stage, as the projectile gradually approaches and then compresses the target, nucleons in the target with a momentum of more than k_F have a greater probability to be accelerated into the region of momentum greater than approximately 600 MeV/c. For this reason, we observe the larger emission rate before approximately 27 fm/c in collisions for the scenario with more SRC nucleons in the colliding nuclei in panel (b) of Fig. 3. For the SRC scenario, with the emission of more preequilibrium nucleons at the early reaction stage, the remainders are naturally less than those in collisions without the consideration of SRCs. Consequently, for the later reaction stages, the nucleon emission rate in collisions without SRCs will dominate, compared with those in collisions with SRCs. Indeed, for the nucleon emission after approximately 27 fm/c, the smaller emission rate is seen in the scenario with more SRC nucleons in the colliding nuclei, as shown in panel (b) of Fig. 3. Moreover, before and/or even at 15 fm/c, we

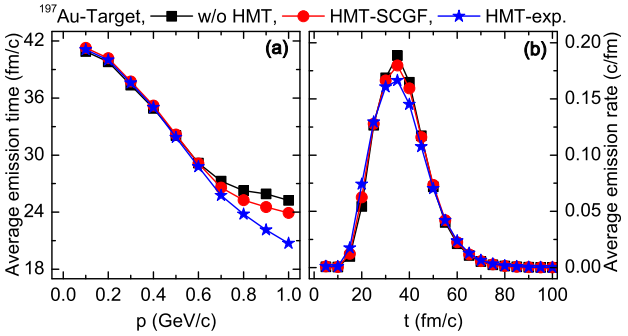

Fig. 3 (Color online) Average **a** emission time and **b** emission rate for nucleons in scenarios with and without the consideration of SRCs. The soft symmetry energy with parameter $x = 1$ is used

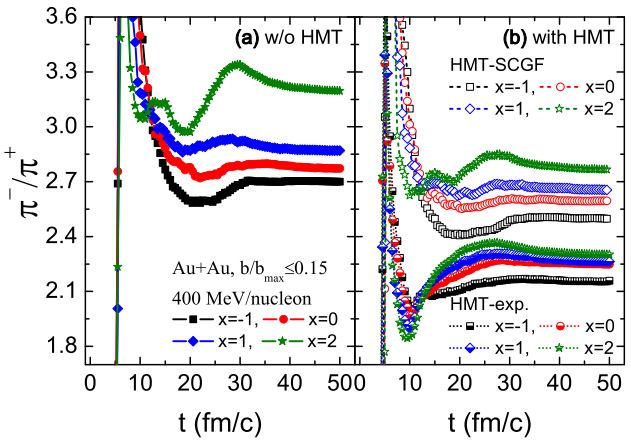

Fig. 4 (Color online) Time evolutions of the $(\pi^-/\pi^+)_{\rm like}$ ratios in central ^{197}Au + ^{197}Au collisions at 400 MeV/nucleon, with the symmetry energy ranging from the superhard with $x = -1$ to the supersoft with $x = 2$. The panels **a** and **b** are the results in scenarios without and with the consideration of SRCs, respectively

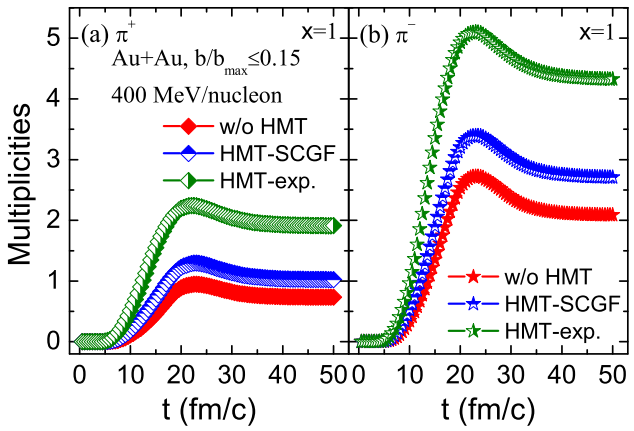

Fig. 5 (Color online) Multiplicities evolutions of dynamic **a** π^+ and **b** π^- in central ^{197}Au + ^{197}Au collisions at 400 MeV/nucleon, in scenarios with and without the consideration of SRCs. The soft symmetry energy with parameter $x = 1$ is used

can observe that the nucleon emission rate is not more than 2.5%; the stability of the ground states at this level, therefore, guarantees that the statistical results obtained here sufficient.

We now verify the influences of SRCs on the final reaction products in ^{197}Au + ^{197}Au collisions. First, we examine the effects of the SRCs on the pion observable. To this end, the dynamic ratio $(\pi^-/\pi^+)_{\rm like}$ defined as

$$(\pi^-/\pi^+)_{\rm like} \equiv \frac{\pi^- + \Delta^- + \frac{1}{3}\Delta^0}{\pi^+ + \Delta^{++} + \frac{1}{3}\Delta^+}, \tag{11}$$

can be used to check the effects of SRCs on the dynamic production of pions. The dynamic ratio $(\pi^-/\pi^+)_{\rm like}$ will naturally become the free π^-/π^+ ratio at the end of the reactions because all the Δ resonances will decay into nucleons and pions. Shown in Fig. 4 are the time evolutions of the dynamic ratios $(\pi^-/\pi^+)_{\rm like}$ in central ^{197}Au + ^{197}Au collisions at 400 MeV/nucleon, with and without the consideration of SRCs. First, it can be observed that without the consideration of SRCs, the dynamic ratio $(\pi^-/\pi^+)_{\rm like}$ during reactions, and thus, the π^-/π^+ ratio at the end of reactions, are generally larger than those with the consideration of SRCs, regardless of the HMT-SCGF parameter or the HMT-exp. parameter is used in calculations. Second, consistent with the established systematics for pion productions [44], it can be found that the π^-/π^+ ratio is indeed sensitive to the density-dependent nuclear symmetry energy $E_{\rm sym}(\rho)$. However, we can also observe a decreased sensitivity of the π^-/π^+ ratio to the nuclear symmetry energy, with the consideration of SRCs, and this phenomenon is more apparent for the case with the HMT-exp. parameter. This observation can be easily understood within the consensus reached about the SRC nucleons in the HMT. Due to the *np* dominance of SRC-nucleon pairs in the HMT [19–22], the higher fraction of SRC nucleons in the HMT naturally leads to more *np* pairs in the reaction system, thus causing further reduction of the isospin asymmetry of the reaction system. Naturally, the dynamic ratio $(\pi^-/\pi^+)_{\rm like}$ during reactions, i.e., the final π^-/π^+ ratio show a decreased sensitivity to the nuclear symmetry energy. To understand the first observation, we should consider the dynamic multiplicities of π^- and π^+ in a quantitative manner shown in the following discussion.

Shown in Fig. 5 are the multiplicities evolutions of dynamic π^- and π^+, with a particular symmetry energy, with parameter $x = 1$ in the same reaction, which are determined by $\pi^- + \Delta^- + \frac{1}{3}\Delta^0$ and $\pi^+ + \Delta^{++} + \frac{1}{3}\Delta^+$, according to the decay mechanism of Δ resonances. The observation of more π^- and π^+ produced in scenarios with the consideration of SRCs is expected, as opposed to without the consideration of SRCs. Consequently, the dynamic ratio $(\pi^-/\pi^+)_{\rm like}$ during reactions, and thus, the final π^-/π^+ ratio, may alter to different extents, according to the specific fraction of SRC nucleons. More specifically, according to the following formula

$$R \equiv \frac{|(\pi^\pm)_{\rm with} - (\pi^\pm)_{\rm w/o}|}{\left[(\pi^\pm)_{\rm with} + (\pi^\pm)_{\rm w/o}\right]/2} \times 100\%, \tag{12}$$

, we can calculate the relative effects of SRCs on the final multiplicities of π^- and π^+; the corresponding results employing the HMT-exp. parameter and the HMT-SCGF parameter are shown in Fig. 6. The figure shows that regardless of whether the HMT-SCGF parameter or the HMT-exp. parameter is used in calculations, the increment of π^+ is more than that of π^-, leading to a corresponding

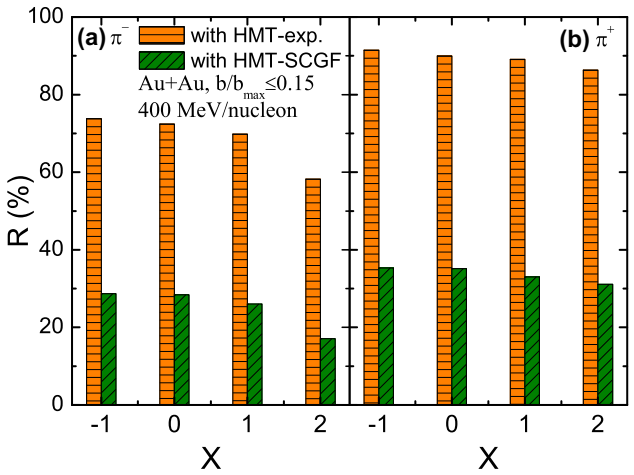

Fig. 6 (Color online) Relative effects of the SRCs on the final multiplicities of **a** π^- and **b** π^+ in central ^{197}Au + ^{197}Au collisions at 400 MeV/nucleon

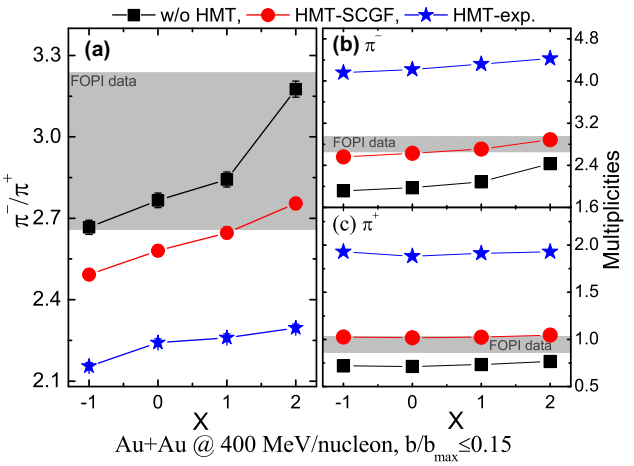

Fig. 7 (Color online) Final multiplicities of π^- and π^+ and the corresponding π^-/π^+ ratios, compared with those from the FOPI experiment in central ^{197}Au + ^{197}Au collisions at 400 MeV/nucleon, without and with the consideration of SRCs

reduction of the π^-/π^+ ratio. This is why we observe the π^-/π^+ ratio generally decreasing in scenarios with the consideration of SRCs in Fig. 4. One may suspect why the increment of π^+ is more than that of π^- in reactions for particular parameter settings. Similar to the above discussion, owing to the *np* dominance of SRC-nucleon pairs, which results in larger probabilities of protons than neutrons in the HMT in neutron-rich systems, more energetic proton–proton collisions can cause more π^+ productions. Naturally, compared to the case with the HMT-SCGF parameter, the case with the HMT-exp. parameter can lead to more high-momentum nucleons in the colliding nuclei, and thus, a greater increment of π^+ than π^-, and more *np* pairs. For this reason, the corresponding π^-/π^+ ratio has smaller values and a weaker sensitivity to the nuclear symmetry energy.

Before investigating the effects of SRCs on the collective flow of nucleons, we first compare the final multiplicities of π^- and π^+ and their π^-/π^+ ratios with the available data to examine the reliability of this isospin-dependent single NMD and the two corresponding sets of parameters for the IANM. Shown in panels (b) and (c) of Fig. 7 are the final multiplicities of π^- and π^+, generated in central ^{197}Au + ^{197}Au collisions for the scenarios with SRCs and those from the FOPI experiment [44]. As a comparison, we also display the corresponding results of central ^{197}Au + ^{197}Au collisions for the scenario without SRCs. Without the consideration of SRCs, the multiplicities of both π^- and π^+ are significantly underestimated in calculations with all x parameters used here; on the contrary, the multiplicities of both π^- and π^+ are significantly overestimated in calculations using the HMT-exp. Parameter. However, for the case using the HMT-SCGF parameter, the theoretical simulations of the ^{197}Au + ^{197}Au collisions can reproduce the multiplicities of both π^- and π^+ of the FOPI experiment, with the symmetry energy parameter x setting approximately in the range from 0–2. To reduce the systematic errors in probing the symmetry energy using the multiplicities of charged pions, their ratios π^-/π^+ are typically used as a more effective observable of the symmetry energy in HICs at intermediate energies. Therefore, panel (a) of Fig. 7 shows the ratios π^-/π^+ of charged pions from the FOPI experiments [44] and the corresponding theoretical simulations in the same reactions, with and without the consideration of SRCs. It can be clearly observed that the theoretical simulations of the ^{197}Au + ^{197}Au collisions, using the HMT-SCGF parameter, can effectively reproduce the π^-/π^+ ratio of the FOPI data under the symmetry energy setting, in a range of parameter x no less than 1. Therefore, from the consistencies of both pion multiplicities, and their ratios, in theoretical simulations using the HMT-SCGF parameter with the FOPI experimental data, we can conclude that this isospin-dependent single NMD given in Eq. (1), and the corresponding HMT-SCGF parameter are reliable for the IANM. Correspondingly, this result also qualitatively favors a mildly soft prediction for the nuclear symmetry energy at high densities. One can also observe that without the consideration of SRCs, the ratio π^-/π^+ of charged pions can also reproduce the FOPI experimental data, even with all x parameters used here. However, it needs to be emphasized that the multiplicities of both π^- and π^+ in this case deviate too far from the FOPI experimental data.

We now investigate the effects of the SRCs on the collective flows of the nucleons. As a typical collective flow, the elliptic flows of nucleons defined as

$$v_2 = \left\langle \frac{p_x^2 - p_y^2}{p_x^2 + p_y^2} \right\rangle, \quad (13)$$

are widely used as the probe of the isovector part of the nuclear interactions in HICs at intermediate energies, and the properties of the hot and dense matter formed in the early stage of HICs at relativistic energies Refs. [45–47]. Presently, predictions on the nuclear symmetry energy using the elliptic flow of nucleons are primarily through comparing theoretical simulations with the available data in FOPI-LAND and/or ASY-EOS experiments [48, 49]. For example, based on these data, the Tübingen quantum-molecular-dynamics (TüQMD) [50] model and ultrarelativistic quantum-molecular-dynamics (UrQMD) [51] model consistently favor a moderately soft prediction for the nuclear symmetry energy at high densities. To extract the precise information about the nuclear symmetry energy using the elliptic flows of the nucleons in HICs, the effect of the SRCs on the elliptic flows of the nucleons must be known. More over, to further verify the reliability of this isospin-dependent NMD and the corresponding parameter settings, we compare our theoretical simulations of the elliptic flows of the nucleons with those from the experiment in the FOPI-LAND collaboration [48, 50], examining the effects of the SRCs on the elliptic flows of the nucleons. Shown in Fig. 8 are the elliptic flows of the nucleons in the semicentral ^{197}Au + ^{197}Au collisions, with an impact parameter $b = 7.2$fm and a beam energy of 400 MeV/nucleon. With the consideration of SRCs, the squeezed out elliptic flows of both neutrons and protons are decreased because the correlations enhance the difficulties of anisotropic nucleons emissions; this phenomenon is especially apparent for the scenario using the HMT-exp. Parameter, due to the stronger correlation effects in this scenario. Again, because the dominance of the *np* SRC pairs reduces the isospin asymmetry of reaction systems, we can also observe a reduced sensitivity of the elliptic flows to the nuclear symmetry energy. Moreover, it can be observed that the elliptic flows of the protons in the FOPI-LAND experiment were not reproduced in our theoretical simulations, regardless of using the HMT-SCGF parameter or the HMT-exp. parameter. Interestingly, it is observed that with the symmetry energy set in a range with parameter x no less than approximately 0.9, the elliptic flows of the neutrons in the FOPI-LAND experiment can be well reproduced by the theoretical simulations of the ^{197}Au + ^{197}Au collisions employing the HMT-exp. Parameter. This constraint on the symmetry energy coincides qualitatively with the previous predictions, using the TüQMD [50] and UrQMD [51] models. Consequently, it can be concluded from this result that the HMT-exp. parameter should not be excluded at present. Finally, similar to the ratio π^-/π^+ of charged pions, the ratio of the neutron elliptic flow over the proton elliptic flow v_2^n/v_2^p is also effective in probing the symmetry energy in HICs. Therefore, we show this ratio in the same reaction in Fig. 9. It can be observed that, by setting the symmetry energy in a range with parameter x no more than approximately 1, the ratio v_2^n/v_2^p in the FOPI-LAND experiment can be well reproduced by theoretical simulations of the ^{197}Au + ^{197}Au collisions in all scenarios, with or without the consideration of SRCs. Moreover, even for all x parameters used here, the theoretical simulations of the ^{197}Au + ^{197}Au collisions using the HMT-exp.

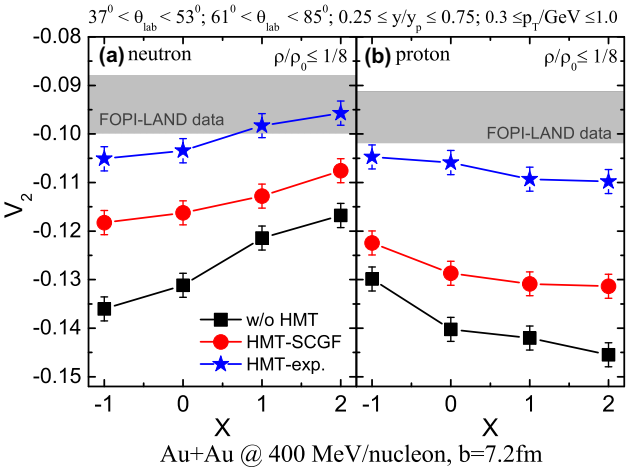

Fig. 8 (Color online) Elliptic flows of **a** neutrons and **b** protons, compared with those from the FOPI-LAND experiment in semicentral ^{197}Au + ^{197}Au collisions, with an impact parameter $b = 7.2$fm at 400 MeV/nucleon, with and without the consideration of SRCs

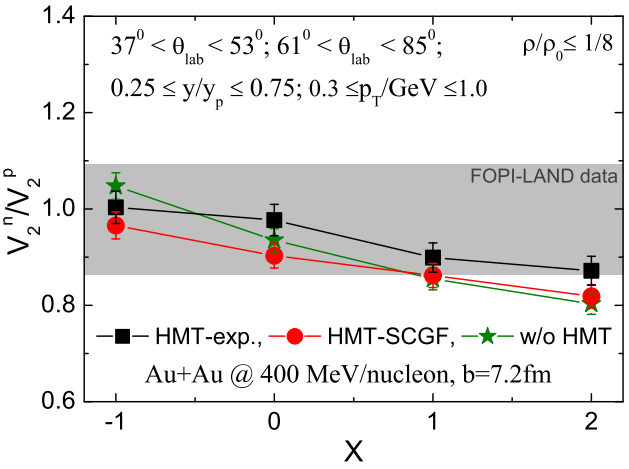

Fig. 9 (Color online) Ratios of neutron elliptic flows over proton elliptic flows, compared with those from the FOPI-LAND experiment in semicentral ^{197}Au + ^{197}Au collisions, with an impact parameter $b = 7.2$ fm at 400 MeV/nucleon, with and without the consideration of SRCs

parameter can well reproduce this ratio of the FOPI-LAND experiment. Similarly, this implies that we should not exclude the HMT-exp. parameter at present. However, considering that the elliptic flows of the protons in these cases do not fit the FOPI-LAND experimental data, we naturally cannot put stringent constraints on the high-density symmetry energy, according to the results from the elliptic flow signals in this study.

Thus far, from the elliptic flow signals and the pion signals obtained above, we can conclude two points: First, the parameterized isospin-dependent single NMD given in Eq. (1) is reliable for the IANM and both the HMT-SCGF parameter and the HMT-exp. parameter cannot be excluded, according to the available experimental information at present; second, according to the pion signals of the theoretical simulations using the HMT-SCGF parameter and their comparisons with the FOPI experimental data, we can make a mildly soft conclusion for the nuclear symmetry energy at high densities. However, our theoretical simulations of the ^{197}Au + ^{197}Au collisions, using both HMT-SCGF and HMT-exp. Parameters, cannot fit the experimental pion data and the experimental elliptic flow data simultaneously; we, therefore, cannot put stringent constraints on the high-density symmetry energy.

4 Summary

Within an IBUU transport model, using nucleon momentum profiles from an isospin-dependent single NMD as the input, with an HMT induced by SRCs, we have investigated the effects of the SRCs on the pion and flow observables in ^{197}Au + ^{197}Au collisions at 400 MeV/nucleon. Compared to the case without the SRCs, the SRCs cause a greater increment of π^+ than π^- in the ^{197}Au + ^{197}Au collisions, leading to a significant reduction of the π^-/π^+ ratio; however, for the flow observables, the SRCs decrease the squeezed out elliptic flows of both neutrons and protons, owing to the correlations, which enhance the difficulties of the anisotropic emission of nucleons. Moreover, owing to the dominance of *np* SRC pairs in the HMT, and thus, a corresponding reduction of the isospin asymmetry of the reaction systems, both pion and flow observables show a reduced sensitivity to the nuclear symmetry energy. However, by comparing the pion and flow observables with the available data, we have also checked the reliability of the used isospin-dependent single NMD and the two corresponding sets of parameters. The theoretical simulation of the ^{197}Au + ^{197}Au collisions, using the HMT-exp. parameter, and the HMT-SCGF parameter can reproduce the neutron elliptic flows of the FOPI-LAND experiment and the π^-/π^+ ratios of the FOPI experiment, respectively, under the symmetry energy setting in a particular range. Therefore, we can conclude that this parameterized isospin-dependent single NMD is reliable for the IANM and both the HMT-SCGF parameter and the HMT-exp. parameter cannot be excluded, according to the available experimental information at present. On the contrary, because our theoretical simulations of the ^{197}Au + ^{197}Au collisions cannot fit the experimental pion data and the experimental elliptic flow data simultaneously, we cannot put stringent constraints on the high-density symmetry energy. However, our study explicitly indicates that the cross examinations of various observables using various experimental data are the necessary solution for the determination of nuclear symmetry energy. Furthermore, the symmetry energy measurement experiment at RIBF-RIKEN in Japan [10], using the SAMURAI-Time-Project-Chamber [52] advance the determination of nuclear symmetry energy at high densities.

Acknowledgements G. F. Wei would like to thank Profs. Gao-Chan Yong and Bao-An Li for helpful discussions.

References

1. J.M. Lattimer, The Nuclear equation of state and neutron star masses. Annu. Rev. Nucl. Part. Sci. **62**, 485 (2012). https://doi.org/10.1146/annurev-nucl-102711-095018
2. C.J. Horowitz, E.F. Brown, Y. Kim et al., A way forward in the study of the symmetry energy: experiment, theory, and observation. J. Phys. G Nucl. Part. Phys. **41**, 093001 (2014). https://doi.org/10.1088/0954-3899/41/9/093001
3. Z.G. Xiao, B.A. Li, L.W. Chen et al., Circumstantial evidence for a soft nuclear symmetry energy at suprasaturation densities. Phys. Rev. Lett. **102**, 062502 (2009). https://doi.org/10.1103/PhysRevLett.102.062502
4. W.J. Xie, J. Su, L. Zhu et al., Symmetry energy and pion production in the Boltzmann–Langevin approach. Phys. Lett. B **718**, 1510 (2013). https://doi.org/10.1016/j.physletb.2012.12.021
5. Z.Q. Feng, G.M. Jin, Probing high-density behavior of symmetry energy from pion emission in heavy-ion collisions. Phys. Lett. B **683**, 140 (2010). https://doi.org/10.1016/j.physletb.2009.12.006
6. N.B. Zhang, B.A. Li, Astrophysical constraints on a parametric equation of state for neutron-rich nucleonic matter. Nucl. Sci. Tech. **29**, 178 (2018). https://doi.org/10.1007/s41365-018-0515-9
7. T.Z. Yan, S. Li, Y.N. Wang et al., Yield ratios and directed flows of light particles from proton-rich nuclei-induced collisions. Nucl. Sci. Tech. **30**, 15 (2019). https://doi.org/10.1007/s41365-018-0534-6
8. M.B. Tsang, J. Estee, H. Setiawan et al., Pion production in rare-isotope collisions. Phys. Rev. C **95**, 044614 (2017). https://doi.org/10.1103/PhysRevC.95.044614
9. Y.X. Zhang, M.B. Tsang, Z.X. Li, Covariance analysis of symmetry energy observables from heavy ion collision. Phys. Lett. B **749**, 262 (2015). https://doi.org/10.1016/j.physletb.2015.07.064
10. Symmetry energy project. http://groups.nscl.msu.edu/hira/sep.htm. Accessed 13 June 2016
11. J. Hong, P. Danielewicz, Subthreshold pion production within a transport description of central Au + Au collisions. Phys. Rev. C **90**, 024605 (2014). https://doi.org/10.1103/PhysRevC.90.024605

12. W.M. Guo, G.C. Yong, H. Liu et al., Effects of pion potential and nuclear symmetry energy on the π^-/π^+ ratio in heavy-ion collisions at beam energies around the pion production threshold. Phys. Rev. C **91**, 054616 (2015). https://doi.org/10.1103/PhysRevC.91.054616
13. Z.Q. Feng, Nuclear dynamics and particle production near threshold energies in heavy-ion collisions. Nucl. Sci. Tech. **29**, 40 (2018). https://doi.org/10.1007/s41365-018-0379-z
14. B.A. Li, Symmetry potential of the $\Delta(1232)$ resonance and its effects on the π^-/π^+ ratio in heavy-ion collisions near the pion-production threshold. Phys. Rev. C **92**, 034603 (2015). https://doi.org/10.1103/PhysRevC.92.034603
15. W.M. Guo, G.C. Yong, W. Zuo, Effect of Δ potential on the π^-/π^+ ratio in heavy-ion collisions at intermediate energies. Phys. Rev. C **92**, 054619 (2015). https://doi.org/10.1103/PhysRevC.92.054619
16. R. Subedi, R. Shneor, P. Monaghan et al., Probing cold dense nuclear matter. Science **320**, 1476 (2008). https://doi.org/10.1126/science.1156675
17. C. Ciofi degli Atti, In-medium short-range dynamics of nucleons: recent theoretical and experimental advances. Phys. Rep. **590**, 1 (2015). https://doi.org/10.1016/j.physrep.2015.06.002
18. B.A. Li, B.J. Cai, L.W. Chen et al., Isospin dependence of nucleon effective masses in neutron-rich matter. Nucl. Sci. Tech. **27**, 141 (2016). https://doi.org/10.1007/s41365-016-0140-4
19. R.B. Wiringa, R. Schiavilla, S.C. Pieper et al., Nucleon and nucleon-pair momentum distributions in $A \leq 12$ nuclei. Phys. Rev. C **89**, 024305 (2014). https://doi.org/10.1103/PhysRevC.89.024305
20. M.M. Sargsian, New properties of the high-momentum distribution of nucleons in asymmetric nuclei. Phys. Rev. C **89**, 034305 (2014). https://doi.org/10.1103/PhysRevC.89.034305
21. J. Ryckebusch, M. Vanhalst, W. Cosyn, Stylized features of single-nucleon momentum distributions. J. Phys. G Nucl. Part. Phys. **42**, 055104 (2015). https://doi.org/10.1088/0954-3899/42/5/055104
22. O. Hen, M. Sargsian, L.B. Weinstein et al., Momentum sharing in imbalanced Fermi systems. Science **346**, 614 (2014). https://doi.org/10.1126/science.1256785
23. M. Duer, O. Hen, E. Piasetzky et al., Probing high-momentum protons and neutrons in neutron-rich nuclei. Nature **560**, 617 (2018). https://doi.org/10.1038/s41586-018-0400-z
24. O. Hen, B.A. Li, W.J. Guo et al., Symmetry energy of nucleonic matter with tensor correlations. Phys. Rev. C **91**, 025803 (2015). https://doi.org/10.1103/PhysRevC.91.025803
25. A. Rios, A. Polls, W.H. Dickhoff, Depletion of the nuclear Fermi sea. Phys. Rev. C **79**, 064308 (2009). https://doi.org/10.1103/PhysRevC.79.064308
26. Z.H. Li, H.J. Schulze, Correlation strength with modern nucleon-nucleon potentials in the Brueckner–Hartree–Fock approach. Phys. Rev. C **94**, 024322 (2016). https://doi.org/10.1103/PhysRevC.94.024322
27. B.J. Cai, B.A. Li, Isospin quartic term in the kinetic energy of neutron-rich nucleonic matter. Phys. Rev. C **92**, 011601 (2015). https://doi.org/10.1103/PhysRevC.92.011601
28. B.A. Li, C.B. Das, S.D. Gupta et al., Momentum dependence of the symmetry potential and nuclear reactions induced by neutron-rich nuclei at RIA. Phys. Rev. C **69**, 011603(R) (2004). https://doi.org/10.1103/PhysRevC.69.011603
29. L. Viverit, S. Giorgini, L.P. Pitaevskii et al., Momentum distribution of a trapped Fermi gas with large scattering length. Phys. Rev. A **69**, 013607 (2004). https://doi.org/10.1103/PhysRevA.69.013607
30. A. Rios, A. Polls, W.H. Dickhoff, Density and isospin-asymmetry dependence of high-momentum components. Phys. Rev. C **89**, 044303 (2014). https://doi.org/10.1103/PhysRevC.89.044303
31. G.F. Wei, B.A. Li, G.C. Yong et al., Effects of retarded electrical fields on observables sensitive to the high-density behavior of the nuclear symmetry energy in heavy-ion collisions at intermediate energies. Phys. Rev. C **97**, 034620 (2018). https://doi.org/10.1103/PhysRevC.97.034620
32. G.F. Wei, G.C. Yong, L. Ou et al., Beam-energy dependence of the relativistic retardation effects of electrical fields on the π^-/π^+ ratio in heavy-ion collisions. Phys. Rev. C **98**, 024618 (2018). https://doi.org/10.1103/PhysRevC.98.024618
33. L.W. Chen, C.M. Ko, B.A. Li et al., Probing isospin- and momentum-dependent nuclear effective interactions in neutron-rich matter. Eur. Phys. J. A **50**, 29 (2014). https://doi.org/10.1140/epja/i2014-14029-6
34. X.H. Li, W.J. Guo, B.A. Li et al., Neutron-proton effective mass splitting in neutron-rich matter at normal density from analyzing nucleon-nucleus scattering data within an isospin dependent optical model. Phys. Lett. B **743**, 408 (2015). https://doi.org/10.1016/j.physletb.2015.03.005
35. I. Vidaña, A. Polls, C. Providência, Nuclear symmetry energy and the role of the tensor force. Phys. Rev. C **84**, 062801 (2011). https://doi.org/10.1103/PhysRevC.84.062801
36. G.C. Yong, Cross-checking the symmetry energy at high densities. Phys. Rev. C **93**, 044610 (2016). https://doi.org/10.1103/PhysRevC.93.044610
37. G.F. Wei, X.G. Cao, Q.J. Zhi et al., Proton-proton momentum correlation function as a probe of the high momentum tail of the nucleon-momentum distribution. Phys. Rev. C **101**, 014613 (2020). https://doi.org/10.1103/PhysRevC.101.014613
38. L. Ou, B.A. Li, Magnetic effects in heavy-ion collisions at intermediate energies. Phys. Rev. C **84**, 064605 (2011). https://doi.org/10.1103/PhysRevC.84.064605
39. X.G. Deng, Y.G. Ma, Electromagnetic field effects on nucleon transverse momentum for heavy ion collisions around 100 A MeV. Nucl. Sci. Tech. **28**, 182 (2017). https://doi.org/10.1007/s41365-017-0337-1
40. O. Buss, Diploma thesis (2004). https://gibuu.hepforge.org/trac/wiki/Paper#Diplomatheses
41. M. Ericson, T.E.O. Ericson, Optical properties of low-energy pions in nuclei. Ann. Phys. **36**, 323 (1966). https://doi.org/10.1016/0003-4916(66)90302-2
42. C. García-Recio, E. Oset, L.L. Salcedo, S-wave optical potential in pionic atoms. Phys. Rev. C **37**, 194 (1988). https://doi.org/10.1103/PhysRevC.37.194
43. J. Nieves, E. Oset, C. García-Recio, Many-body approach to low-energy pion-nucleus scattering. Nucl. Phys. A **554**, 554 (1993). https://doi.org/10.1016/0375-9474(93)90246-T
44. W. Reisdorf, A. Andronic, R. Averbeck et al., Systematics of central heavy ion collisions in the 1 AGeV regime. Nucl. Phys. A **848**, 366 (2010). https://doi.org/10.1016/j.nuclphysa.2010.09.008
45. P. Danielewicz, R. Lacey, W.G. Lynch, Determination of the equation of state of dense matter. Science **298**, 1592 (2002). https://doi.org/10.1126/science.1078070
46. P.C. Li, Y.J. Wang, Q.F. Li et al., Collective flow and nuclear stopping in heavy ion collisions in Fermi energy domain. Nucl. Sci. Tech. **29**, 177 (2018). https://doi.org/10.1007/s41365-018-0510-1
47. H.C. Song, S.A. Bass, U. Heinz et al., 200 AGeV Au + Au collisions serve a nearly perfect quark-gluon liquid. Phys. Rev. Lett. **106**, 192301 (2011). https://doi.org/10.1103/PhysRevLett.106.192301
48. Y. Leifels, Th Blaich, ThW Elze et al., Exclusive studies of neutron and charged particle emission in collisions of ^{197}Au + ^{197}Au at 400 MeV/nucleon. Phys. Rev. Lett. **71**, 963 (1993). https://doi.org/10.1103/PhysRevLett.71.963

49. P. Russotto, S. Gannon, S. Kupny et al., Results of the ASY-EOS experiment at GSI: The symmetry energy at suprasaturation density. Phys. Rev. C **94**, 034608 (2016). https://doi.org/10.1103/PhysRevC.94.034608
50. M.D. Cozma, Y. Leifels, W. Trautmann et al., Toward a model-independent constraint of the high-density dependence of the symmetry energy. Phys. Rev. C **88**, 044912 (2013). https://doi.org/10.1103/PhysRevC.88.044912
51. W. Trautmann, H.H. Wolter, Elliptic flow and the symmetry energy at supra-saturation density. Int. J. Mod. Phys. E **21**, 1230003 (2012). https://doi.org/10.1142/S0218301312300032
52. R. Shane, A.B. McIntosh, T. Isobe et al., SπRIT: A time-projection chamber for symmetry-energy studies. Nucl. Instrum. Meth. A **784**, 513 (2015). https://doi.org/10.1016/j.nima.2015.01.026